Electronic Supplementary Material (ESI) for Dalton Transactions.
This journal is © The Royal Society of Chemistry 2023

Supporting Information

Exploring a Prototype for Cooperative Structural Phase Transition in Cobalt(II) Spin Crossover Compounds

Yi-Fei Deng, Yi-Nuo Wang, Xin-Hua Zhao, and Yuan-Zhu Zhang*

Department of Chemistry, Southern University of Science and Technology (SUSTech), Shenzhen 518055, China.

Email: zhangyz@sustech.edu.cn

Experimental Section

Materials and Syntheses. N, N'-(ethane-1,2-diyl)bis(1-phenyl-1-(pyridin-2-yl)methanimine) (enbzp) was prepared according to the literature.[1] All other chemicals and reagents were commercially available and used without further purification.

Caution. Although no such issues were observed during the present work, perchlorate salts are potentially explosive and should be handled in small quantities with great care.

Synthesis of {[(enbzp)Co(μ-bpee)](ClO$_4$)$_2$·2MeOH·H$_2$O}$_n$ (1). A methanolic solution (5 ml) containing Co(ClO$_4$)$_2$·6H$_2$O (36.5 mg, 0.1 mmol) and enbzp (39.1 mg, 0.1 mmol) was allowed to stir for 30 min at 45 ^{o}C in an ambient atmosphere. The mixture was filtered after cooling to room temperature, 1, 2-bis(4-pyridyl)ethylene (bpee) (18.2 mg, 0.1 mmol) in 5 mL MeOH was subsequently added into the purple filtrate, and the resulting solution was left to evaporate slowly for about 3 days. The red block crystals were collected by filtration and washed with methanol. Yield 58.4 mg (64%). Anal. Calcd. (Found; %) for $C_{40}H_{42}Cl_2CoN_6O_{11}$: C, 52.64 (52.36); H, 4.64 (4.78); N, 9.21 (9.46). FT-IR data (cm^{-1}): 3547 (w), 3068 (w), 2930 (w), 1604 (s), 1442 (m), 1417 (m), 1356 (w), 1330 (m), 1261 (m), 1219 (w), 1182(w), 1163 (w), 1074 (vs), 976 (m), 827 (m), 790 (m), 744 (m), 702 (s), 682 (w), 665 (w), 619 (vs).

The desolvated sample (**1d)** was obtained by heating the crystalline sample of **1** at 360 K for 1 hour in vacuum. FT-IR data (cm^{-1}): 3558 (w), 3062 (w), 2929 (w), 1599 (s), 1440 (m), 1424 (m), 1352 (w), 1330 (m), 1265 (w), 1216 (w), 1184 (w), 1164 (w), 1076 (vs), 972 (m), 823 (m), 790 (m), 741 (m), 705 (s), 680 (w), 668 (w), 619 (vs). Anal. Calcd. (Found; %) for $C_{38}H_{32}Cl_2CoN_6O_8$ (proposed): C, 54.95 (54.83); H, 3.88 (4.06); N, 10.12 (10.28).

Synthesis of {[(enbzp)Co(μ-bpea)](ClO$_4$)$_2$}$_n$ (2). Compound **2** was obtained in a similar way to compound **1**, by using 1, 2-bis(4-pyridyl)ethane (bpea) instead of bpee ligands. Yield 56.6 mg (68%). Anal. Calcd. (Found; %) for $C_{38}H_{34}Cl_2CoN_6O_8$: C, 54.82 (54.97); H, 4.12 (3.88); N, 10.09 (9.85). FT-IR data (cm^{-1}): 3774 (w), 3065 (w), 2937 (w), 1608 (s), 1442 (m), 1422 (m), 1359 (w), 1332 (w), 1261 (w), 1224 (w), 1163 (w), 1078 (vs), 968 (w), 818 (m), 791 (m), 748 (s), 700 (s), 681 (w), 667 (w), 619 (vs).

Synthesis of [{(enbzp)Co}$_2$(μ-bpee)](ClO$_4$)$_4$·2MeOH (3). A methanolic solution (5 ml) containing Co(ClO$_4$)$_2$·6H$_2$O (36.5 mg, 0.1 mmol) and enbzp (39.1 mg, 0.1 mmol) was allowed to stir for 30 min at 45 ^{o}C in an ambient atmosphere. After cooling to room temperature, the mixture was filtered; 1, 2-bis(4-pyridyl)ethylene (bpee) (9.1 mg, 0.05 mmol) in 5 mL MeOH was subsequently added

into the purple filtrate, and the resulting solution was left to evaporate slowly to yield the red block crystals. The product was collected by filtration and washed with methanol. Yield 40.1 mg (52%). Anal. Calcd. (Found; %) for $C_{66}H_{62}Cl_4Co_2N_{10}O_{18}$: C, 51.38 (51.77); H, 4.05 (3.64); N, 9.08 (9.56). FT-IR data (cm^{-1}): 3748 (w), 3214 (w), 2361 (s), 2339 (m), 2159 (s), 2023 (s), 1973 (s), 1602 (m), 1439 (w), 1330 (m), 1262 (m), 1071 (s), 972 (s), 823 (m), 786 (m), 743 (s), 697 (s), 617 (s).

Synthesis of [{(enbzp)Co}$_2$(μ-bpea)](ClO$_4$)$_4$·2MeOH (4). Compound **4** was obtained in a similar way to compound **3**, by using 1, 2-bis(4-pyridyl)ethane (bpea) instead of bpee ligands. Yield 43.3 mg (56%). Anal. Calcd. (Found; %) for $C_{66}H_{64}Cl_4Co_2N_{10}O_{18}$: C, 51.31 (51.78); H, 4.18 (4.64); N, 9.07 (8.75). FT-IR data (cm^{-1}): 3746 (w), 3218 (w), 2362 (s), 2339 (m), 2161 (s), 2026 (s), 1976 (s), 1606 (m), 1442 (w), 1331 (m), 1267 (m), 1068 (s), 976 (w), 822 (m), 786 (m), 743 (s), 702 (s), 617 (s).

Crystallography. Single crystal X-ray diffraction (SCXRD) data for **1** - **4** were collected using a Bruker D8 VENTURE diffractometer with graphite monochromated Mo Kα radiation (λ = 0.71073 Å). The structures were solved by the direct method[2] of SHELXT structure solution program and refined by full-matrix least squares (SHELXL) on F^2 and empirical absorption corrections[3] (SADABS) were applied. Anisotropic thermal parameters were used for the non-hydrogen atoms. Hydrogen atoms were added geometrically and refined using a riding model. CCDC-2296638 (**1**), 2296639 (**2**), 2296640 (**3**-250 K), 2306702 (**3**-100 K) and 2296641 (**4**) contain the crystallographic data that can be obtained via www.ccdc.cam.ac.uk/conts/retrieving.html (or from the Cambridge Crystallographic Data Centre, 12, Union Road, Cambridge CB21EZ, UK; fax: (+44) 1223-336-033; or deposit@ccdc.cam.ac.uk).

Physical Measurements. Elemental analyses (EA) (C, H, N, S) were measured by a vario electroluminescence (EL) cube CHNOS Elemental Analyzer Elementar Analysensysteme GmbH. Fourier transform infrared spectroscopy (FT-IR) spectra were recorded in the range 600-4000 cm^{-1} using a Bruker TENSOR II spectrophotometer. Thermogravimetric analysis (TGA) experiments were performed with fresh samples using a METTLER TOLEDO TGA2 instrument. The TGA curves were measured under an argon atmosphere from 30 to 500 °C with a heating rate of 5 °C /min. Differential scanning calorimeter (DSC) measurements were recorded at 200-400 K with a temperature scan rate of 10, 5, 3 and 1 K/min, respectively, using a TA Instruments Discovery DSC2500. Powder X-ray diffraction (PXRD) measurements were performed using a Rigaku SmartLab X-ray diffractometer with Cu Kα radiation (45 kV, 200 mA) between 5° and 50°

(2θ). The simulated patterns are calculated based on the single-crystal data. Variable temperature PXRD patterns for **1d** were collected at 370 → 400 K → 200 K with an average scan rate of about 0.63 K/min, taking into account the time decay for both temperature changes and data collection. Magnetic susceptibility data were collected under an applied 1 kOe direct current (dc) field in the temperature range 2 - 400 K using a SQUID MPMS3 magnetometer. In the sweeping mode the magnetic susceptibility data of **1d** were recorded in the temperature range 400-150 K at rates 10, 8, 5, 3 and 1 K/min, respectively. In the settle mode the magnetic data were collected in the temperature range 400 - 150 K with an average scan rate of about 2.3 K/min. For the relaxation experiments of **1d**, the sample was cooled from 400 K to the indicated temperature using a scan rate of 10 K/min, and then the susceptibility data were collected at periodic time intervals. Magnetic data were corrected for the diamagnetism of sample holder; for the diamagnetism of the sample using Pascal's constants.[4]

Table S1. Crystallographic data for **1** and **2**.

Compd.	**1**	**2**
Empirical Formula	$C_{40}H_{42}Cl_2CoN_6O_{11}$	$C_{38}H_{34}Cl_2CoN_6O_8$
Molecular weight /g mol^{-1}	912.62	832.54
Crystal system	Monoclinic	Monoclinic
Space group	$P2_1/n$	$P2_1/c$
a, Å	13.8068(12)	17.7150(15)
b, Å	20.3436(17)	13.7858(13)
c, Å	14.7359(13)	16.3340(15)
α, deg	90	90
β, deg	92.102(3)	105.434(3)
γ, deg	90	90
V, Å^3	4136.2(6)	3845.2(6)
Z	4	4
D_{cal}/g cm^{-3}	1.466	1.438
Temperature, K	150	300
2θ range, deg	4.87-49.48	5.61-49.50
Completeness	99.5%	98.8%
Residual map, e Å^{-3}	1.16/-1.37	0.86/-0.58
Goodness-of-fit on F^2	1.053	1.029
Final indices[I>2σ(I)][a, b]	R_1 = 0.0667, wR_2 = 0.1606	R_1 = 0.0642, wR_2 = 0.1720
R indices (all data)	R_1 = 0.0769, wR_2 = 0.1676	R_1 = 0.0761, wR_2 = 0.1819

[a] $R_1 = \sum \| F_o | - | F_c \| / \left[\sum | F_o | \right]$ [b] $wR_2 = \left[\sum \left[w(F_o^2 - F_c^2)^2 \right] / \sum \left[w(F_o^2)^2 \right] \right]^{1/2}$ $w = 1/\sigma^2(F_o^2) + (aP)^2 + bP$ where $P = \left[\max(0 \text{ or } F_o^2) + 2(F_c^2) \right]/3$

Table S2. Crystallographic data for **3** and **4**.

Compd.		**3**	**4**
Empirical Formula	$C_{66}H_{62}Cl_4Co_2N_{10}O_{18}$	$C_{66}H_{62}Cl_4Co_2N_{10}O_{18}$	$C_{66}H_{64}Cl_4Co_2N_{10}O_{18}$
Molecular weight /g mol^{-1}	1542.91	1542.91	1544.93
Crystal system	Monoclinic	Monoclinic	Monoclinic
Space group	$P2_1/n$	$P2_1/n$	$C2/c$
a, Å	13.2660(18)	14.1227(11)	40.420(5)
b, Å	17.777(2)	14.6411(11)	7.1577(9)
c, Å	15.553(2)	16.7951(13)	24.126(3)
α, deg	90	90	90
β, deg	108.877(6)	104.193(3)	105.011(4)
γ, deg	90	90	90
V, Å^3	3470.7(8)	3366.7(5)	6741.8(14)
Z	2	2	4
D_{cal}/g cm^{-3}	1.476	1.522	1.522
Temperature, K	250	100	250
2θ range, deg	4.90-49.50	5.00-49.50	5.79-49.40
Completeness	98.9%	99.4%	97.4%
Residual map, e Å^{-3}	0.98/-0.78	0.88/-0.56	0.94/-0.86
Goodness-of-fit on F^2	1.084	1.069	1.056
Final indices[I>2σ(I)][a, b]	R_1 = 0.0783, wR_2 = 0.2138	R_1 = 0.0808, wR_2 = 0.1598	R_1 = 0.0597, wR_2 = 0.1595
R indices (all data)	R_1 = 0.0879, wR_2 = 0.2223	R_1 = 0.1173, wR_2 = 0.1739	R_1 = 0.0792, wR_2 = 0.1759

Table S3. Selected bond lengths [Å] and angles [deg] for **1** and **2**.

Compd.	**1**	**2**
Co1-N1	2.007(3)	2.018(3)
Co1-N2	1.873(3)	1.888(3)
Co1-N3	1.876(3)	1.897(3)
Co1-N4	2.002(3)	2.018(3)
Co1-N5	2.204(3)	2.235(3)
Co1-N6A	2.249(3)	2.275(3)
$Co\text{-}N_{average}$	2.035(3)	2.055(3)
C32-C33	1.335(6)	1.485(7)
N1-Co1-N4	111.80(13)	113.35(13)
N1-Co1-N5	85.64(13)	86.21(12)
N1-Co1-N6A	90.16(12)	90.63(12)
N2-Co1-N1	81.70(13)	81.32(13)
N2-Co1-N3	84.82(13)	84.34(13)
N2-Co1-N4	166.06(13)	165.30(13)
N2-Co1-N5	90.72(13)	94.10(12)
N2-Co1-N6A	92.74(12)	87.45(12)
N3-Co1-N1	166.49(13)	165.57(13)
N3-Co1-N4	81.61(13)	81.03(13)
N3-Co1-N5	95.40(12)	93.25(12)
N3-Co1-N6A	89.64(12)	90.33(13)
N4-Co1-N5	93.71(12)	88.15(11)
N4-Co1-N6A	84.03(12)	91.21(12)
N5-Co1-N6A	174.13(12)	176.22(12)

Symmetry transformations used to generate equivalent atoms. **1**: ^{A}1+x, +y, +z; **2**: ^{A}+x, -1+y, +z.

Table S4. Selected bond lengths [Å] and angles [deg] for **3** and **4**.

Compd.	**3** (250 K)	**3** (100 K)	**4**
Co1-N1	1.985(4)	1.952(5)	1.979(3)
Co1-N2	1.872(4)	1.876(5)	1.873(3)
Co1-N3	1.867(4)	1.855(6)	1.860(3)
Co1-N4	1.971(4)	1.985(5)	2.000(3)
Co1-N5	2.113(4)	2.098(5)	2.152(3)
$Co\text{-}N_{average}$	1.962(4)	1.953(5)	1.973(3)
Co1-O7	2.645(8)	2.573(5)	2.584(6)
C32-C32A	1.310(12)	1.238(16)	1.507(9)
N1-Co1-N4	108.81(18)	110.1(2)	110.54(14)
N1-Co1-N5	92.75(17)	91.5(2)	95.38(13)
N2-Co1-N1	81.70(18)	82.1(2)	81.47(14)
N2-Co1-N3	84.87(18)	84.7(2)	85.20(14)
N2-Co1-N4	165.41(18)	155.9(2)	161.33(14)
N2-Co1-N5	96.04(17)	101.3(2)	95.55(13)
N3-Co1-N1	160.69(19)	166.7(2)	166.14(13)
N3-Co1-N4	82.35(18)	81.5(2)	81.49(13)
N3-Co1-N5	102.44(19)	93.1(2)	89.64(13)
N4-Co1-N5	93.57(18)	99.1(2)	97.39(13)

Symmetry transformations used to generate equivalent atoms. **3** (250 K): ^{A}1-x, 2-y, 1-z; **3** (100 K): ^{A}2-x, 1-y, 1-z; **4**: ^{A}1/2-x, 3/2-y, 1-z.

Table S5. Structural distortion parameters of **1** - **4**.

Compd.	Σ_{Co}[a]	$CShM_{Co}$[b]
1	67.10	1.873
2	64.38	1.937
3 (250 K)	64.69	1.648
3 (100 K)	66.80	1.903
4	61.06	1.801

[a] Σ_{Co}: the sum of |90-α| for the *cis*-N-Co-N angles around the cobalt atom; [b] $CShM_{Co}$: the continuous shape measurement relative to ideal octahedron (**1**, **2**) or square pyramid (**3**, **4**) geometry of the Co center.

Table S6. The transition temperatures ($T_{1/2}\downarrow$, cooling; $T_{1/2}\uparrow$, heating) for the thermal hysteresis of **1d** at different scan rates.

scan rate	$T_{1/2}\downarrow$	$T_{1/2}\uparrow$	ΔT	T_{center}
10 K/min		362 K		
8 K/min		362 K		
5 K/min	300 K	358 K	58 K	329 K
3 K/min	302 K	354 K	52 K	328 K
1 K/min	304 K	346 K	42 K	325 K

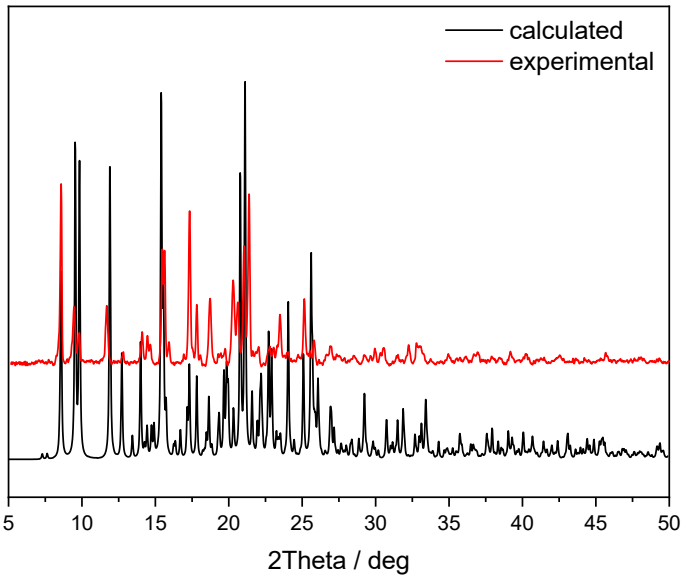

Fig. S1 Powder X-ray diffraction patterns of **1** at room temperature. The calculated patterns are obtained based on the single crystal data of **1** at 150 K.

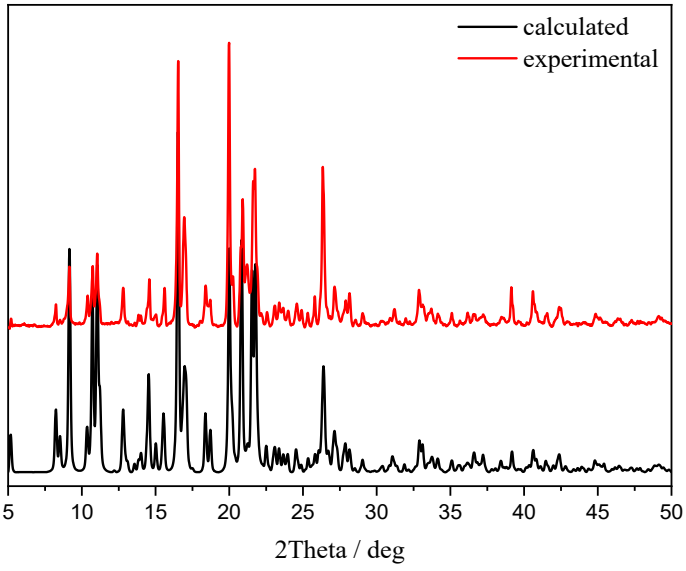

Fig. S2 Powder X-ray diffraction patterns of **2** at room temperature. The calculated patterns are obtained based on the single crystal data of **2** at 300 K.

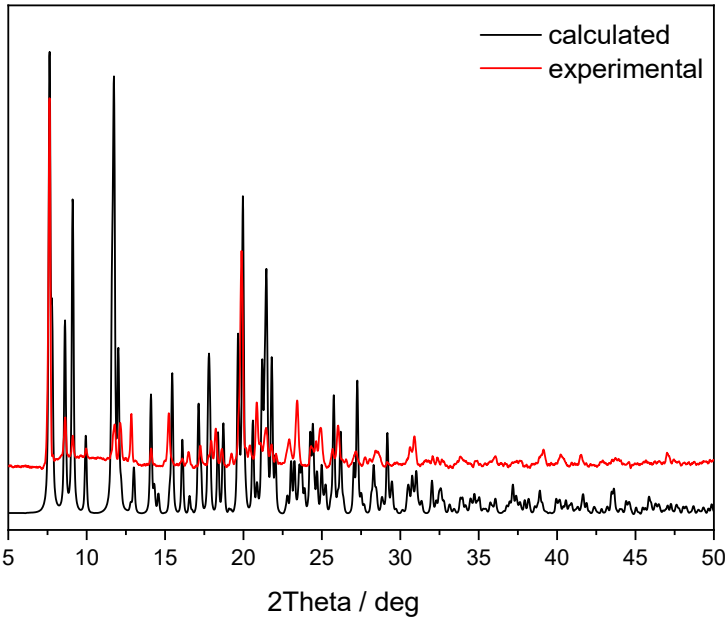

Fig. S3 Powder X-ray diffraction patterns of **3** at room temperature. The calculated patterns are obtained based on the single crystal data of **3** at 250 K.

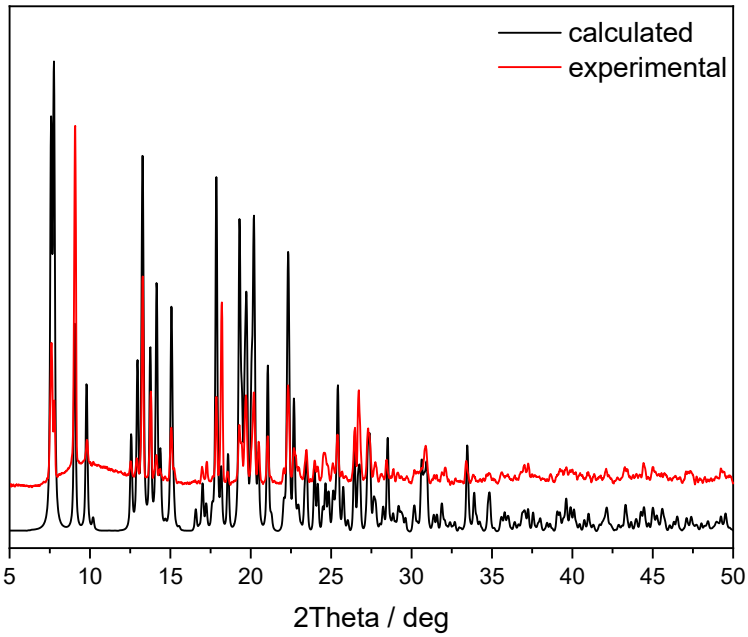

Fig. S4 Powder X-ray diffraction patterns of **4** at room temperature. The calculated patterns are obtained based on the single crystal data of **4** at 250 K.

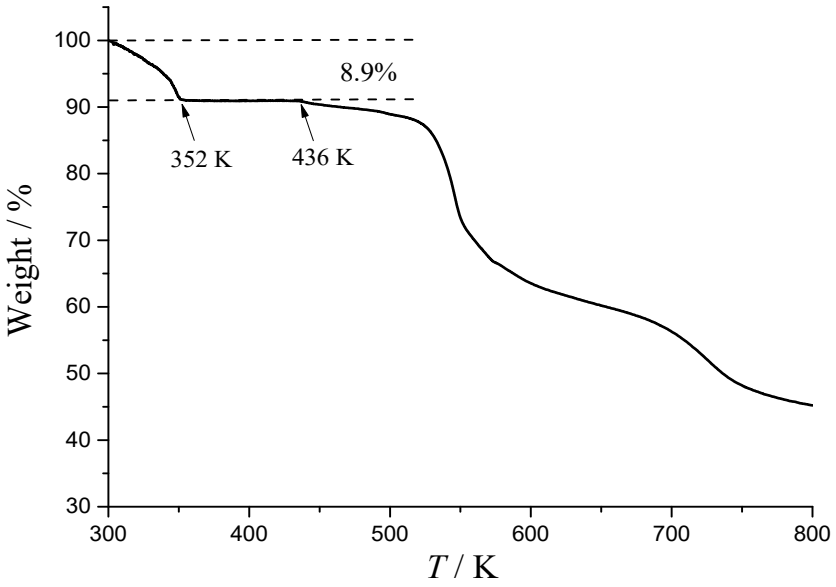

Fig. S5 Thermogravimetric analysis curve of **1**.

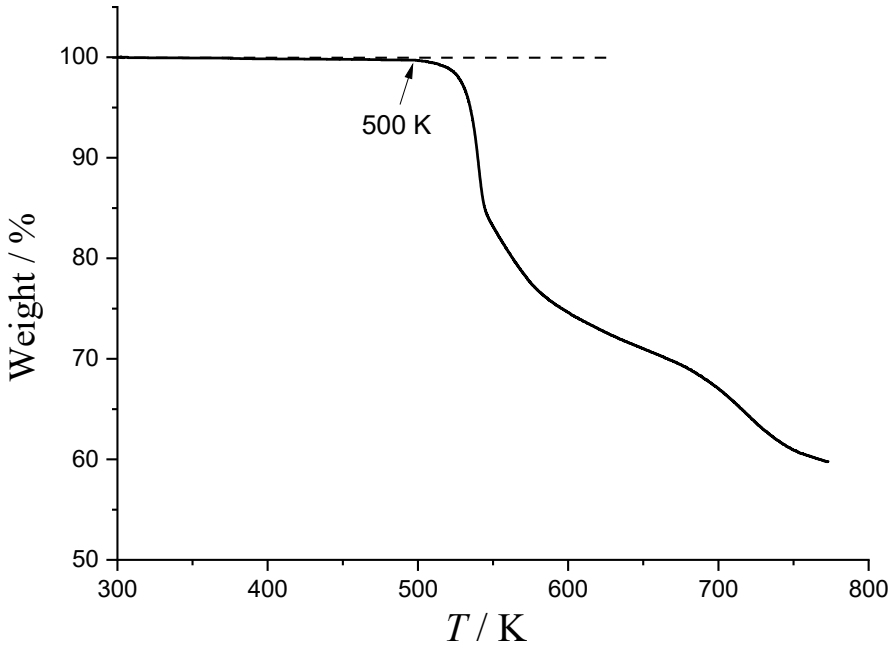

Fig. S6 Thermogravimetric analysis curve of **2**.

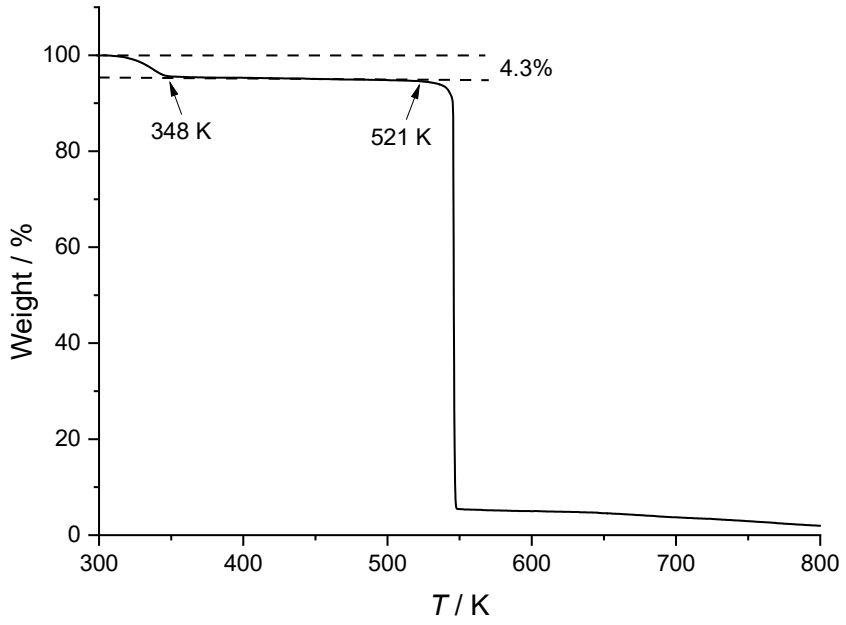

Fig. S7 Thermogravimetric analysis curve of **3**.

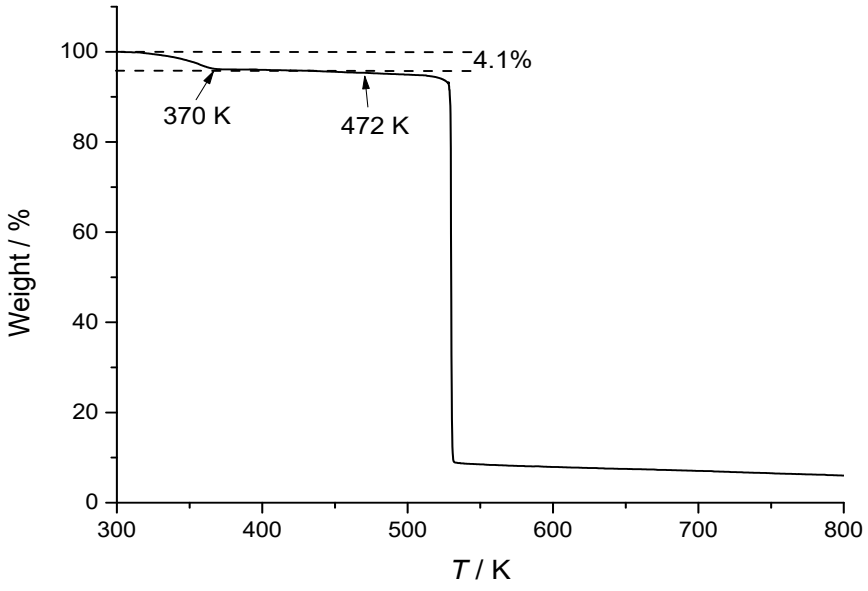

Fig. S8 Thermogravimetric analysis curve of **4**.

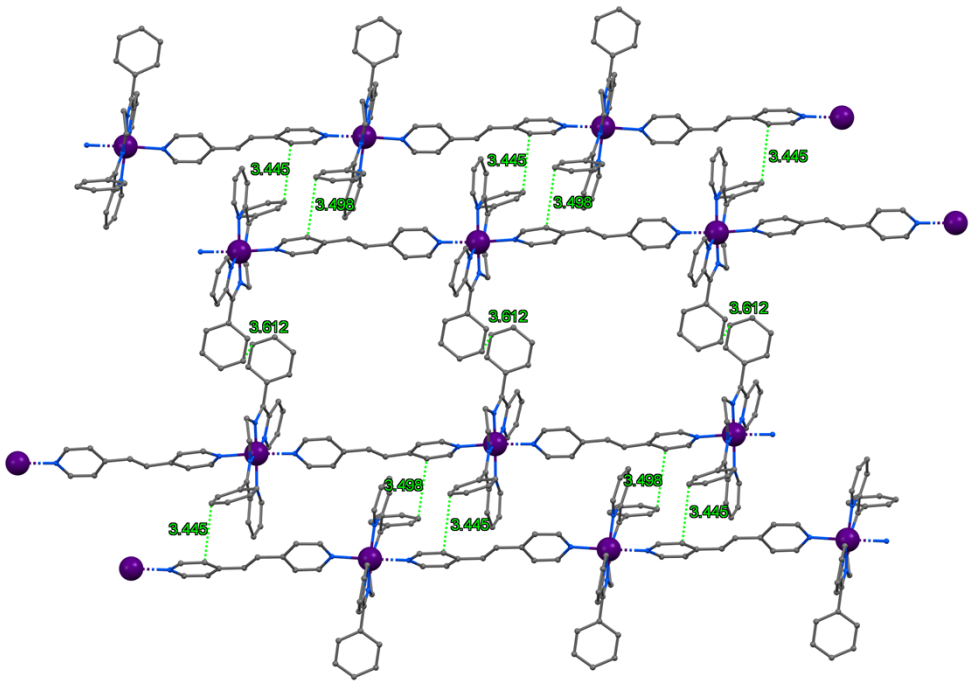

Fig. S9 The packing structure for **1** showing the interchain π···π interactions between enbzp rings (3.612 Å) or between enbzp and bpee ligands (3.445, 3.498 Å). Colour codes: Co, purple; C, grey; N, blue. Lattice solvents, hydrogen atoms and counterions are omitted for clarity.

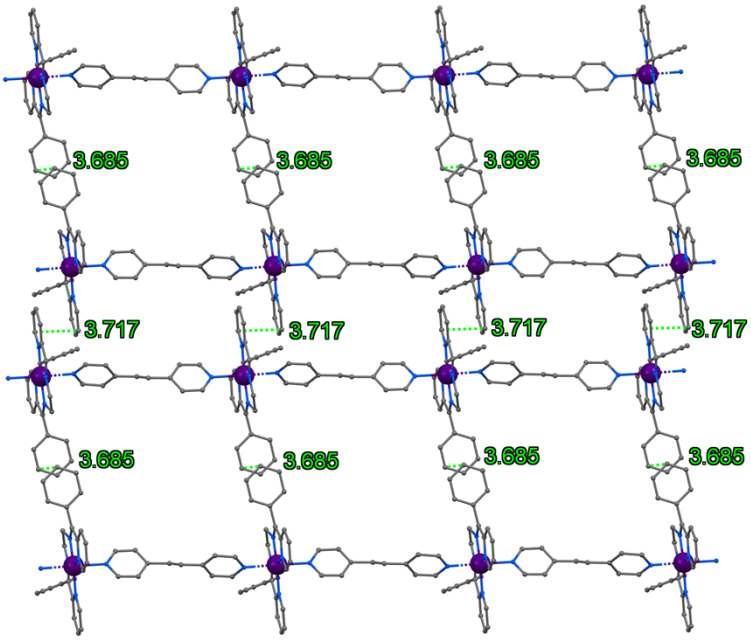

Fig. S10 The packing structure for **2** showing the interchain π···π interactions between the enbzp rings (3.685, 3.717 Å). Colour codes: Co, purple; C, grey; N, blue. Hydrogen atoms, disorders and counterions are omitted for clarity.

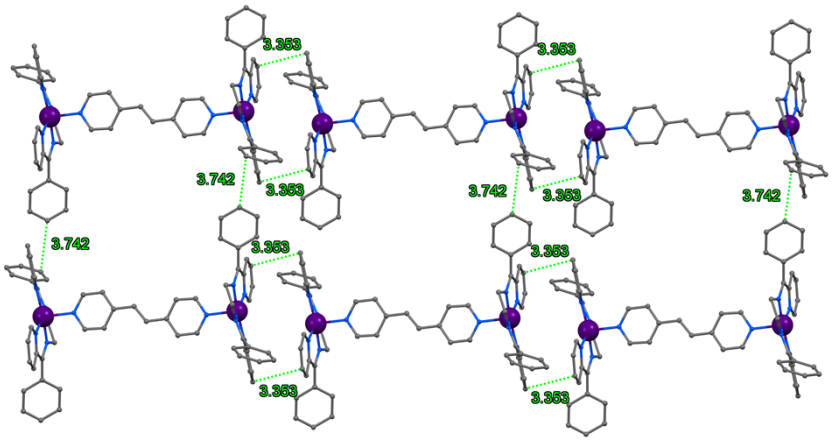

Fig. S11 The packing structure for **3** at 250 K showing the intermolecular π···π interactions between the enbzp rings (3.353, 3.742 Å). Colour codes: Co, purple; C, grey; N, blue. Lattice solvents, hydrogen atoms and counterions are omitted for clarity.

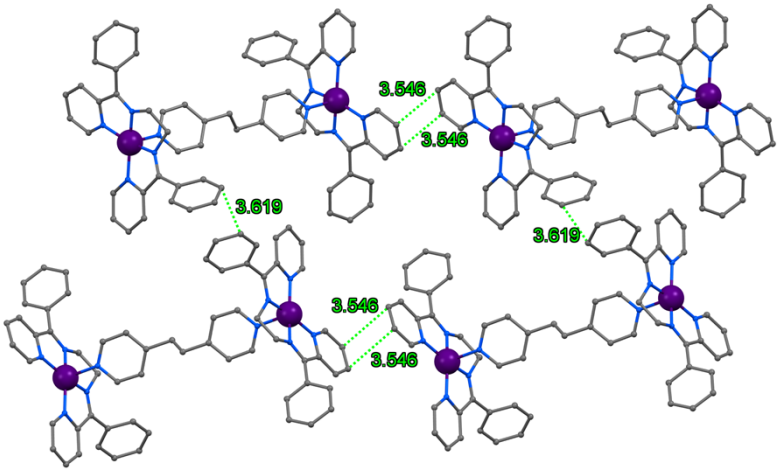

Fig. S12 The packing structure for **4** showing the inter-chain π···π interactions between the enbzp rings (3.546, 3.619 Å). Colour codes: Co, purple; C, grey; N, blue. Lattice solvents, hydrogen atoms and counterions are omitted for clarity.

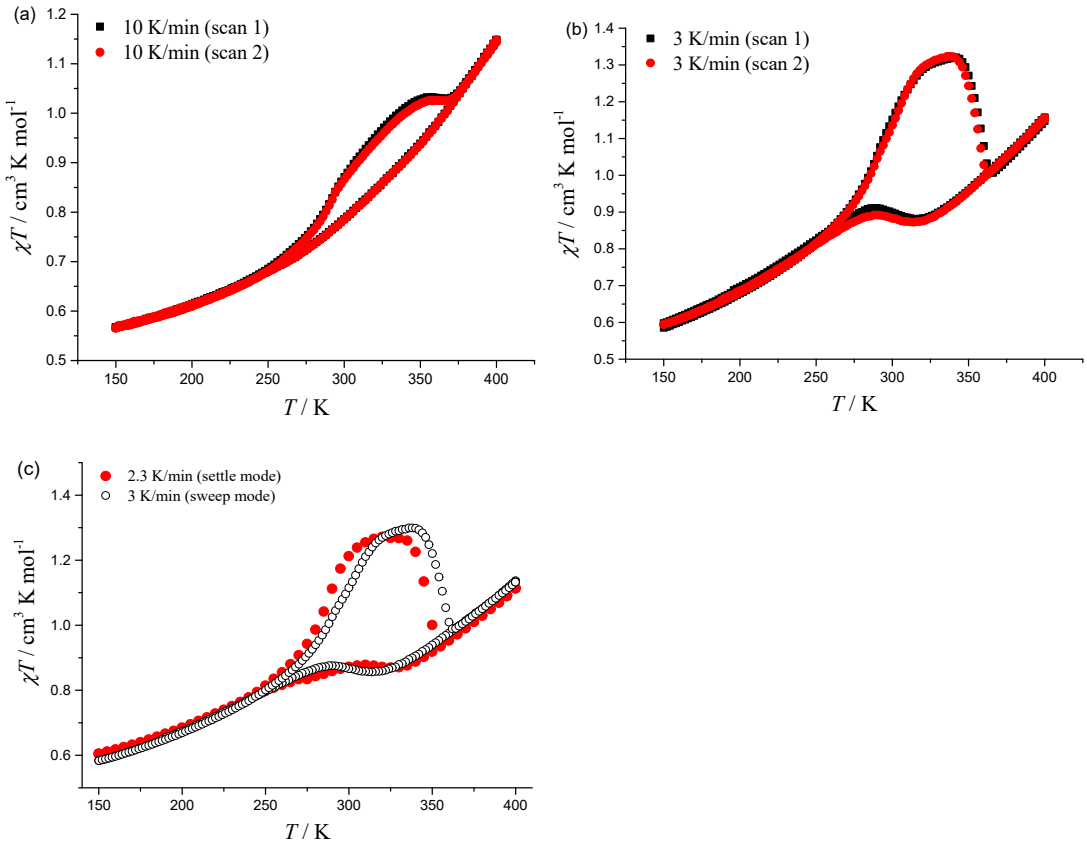

Fig. S13 χT vs. T plots for **1d** in sweep mode scanning at 10 (a) and 3 K/min (b), and in settle mode scanning at about 2.3 K/min (c), respectively.

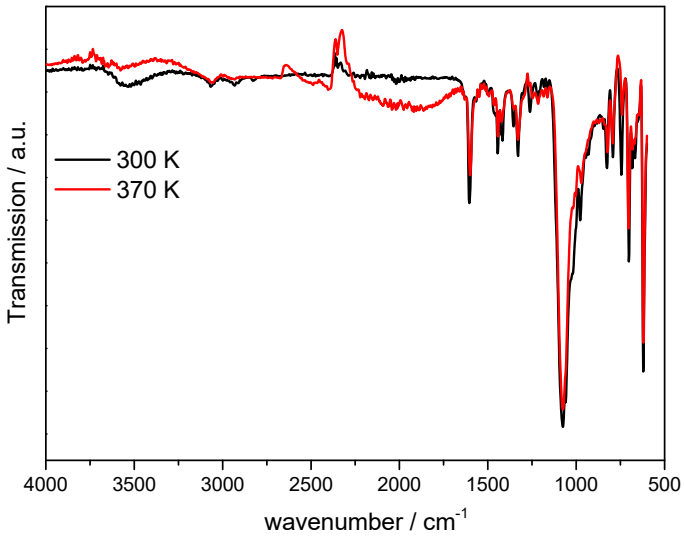

Fig. S14 Variable temperature infrared spectra for **1** at 300 K and **1d** at 370 K.

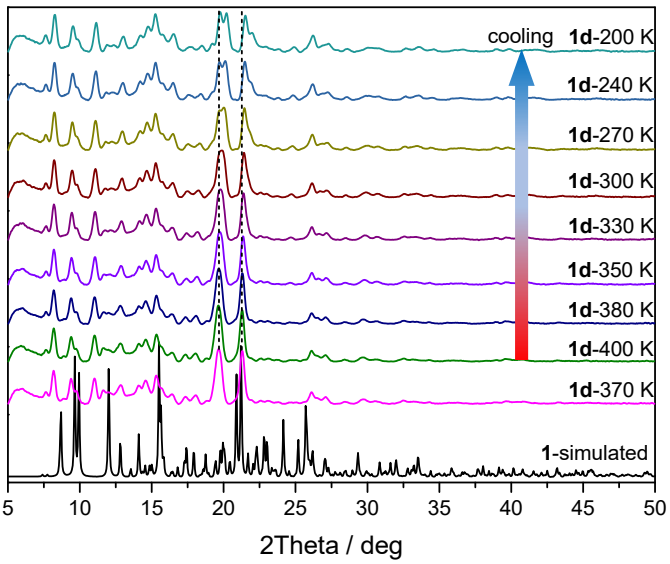

Fig. S15 Variable temperature PXRD patterns for **1d** recorded at 370 → 400 K → 200 K. The simulated pattern for **1** is calculated based on the single crystal data at 150 K.

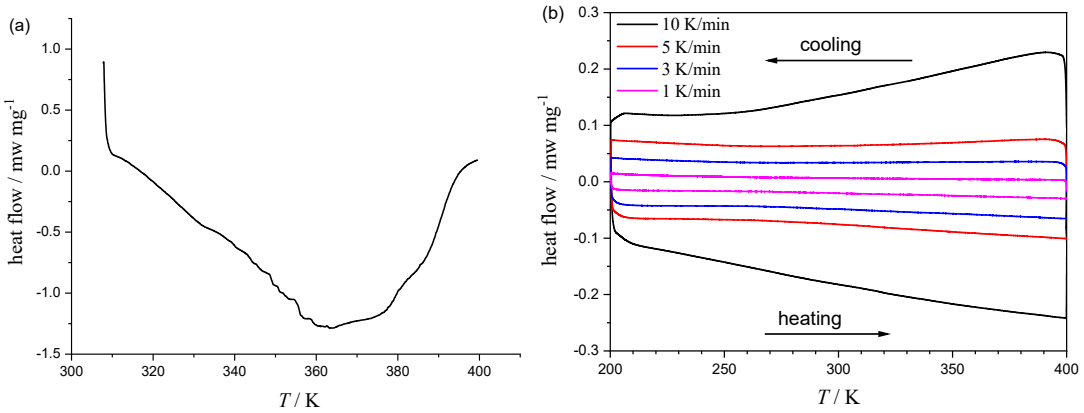

Fig. S16 DSC plots of **1** at 300 - 400 K (a), and **1d** recorded at 200 K - 400 K (b) with different sweep rates.

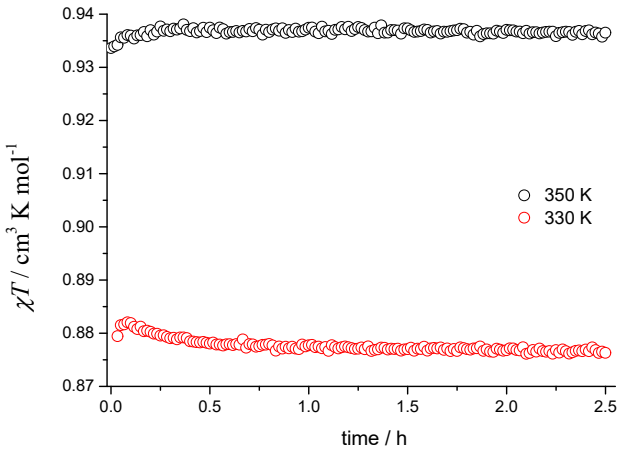

Fig. S17 Time dependence of magnetic susceptibility for **1d** at 350 and 330 K.

Reference

1. T. K. Karmakar, S. K. Chandra, J. Ribas, G. Mostafa, T. H. Lu and B. K. Ghosh, Synthesis, structure and magnetism of a new dicubane-like ferromagnetic tetranuclear nickel cluster containing versatile azido-only bridges and a bis(bidentate) Schiff base blocker, *Chem. Commun.*, 2002, 2364-2365.
2. G. M. Sheldrick, SHELXL-2014, Program for the solution of crystal structures. *University of Göttingen, Göttingen, Germany* 2014.
3. G. M. Sheldrick, SADABS, v.2.01, Bruker/Siemens Area Detector Absorption Correction Program. Bruker AXS: Madison. *Wisconism* 1998.
4. G. A. Bain and J. F. Berry, Diamagnetic Corrections and Pascal's Constants, *J. Chem. Educ.* 2008, **85**, 532-536.